

CAFOSat: A Strongly Annotated Dataset for Infrastructure-Aware CAFO Mapping Using High-Resolution Imagery

Oishee Bintey Hoque^{*,1}, Nibir Chandra Mandal^{*,1}, Mandy L Wilson², Samarth Swarup²,
Madhav Marathe^{1,2}, Abhijin Adiga²

¹University of Virginia ²Biocomplexity Institute, University of Virginia

oishee@virginia.edu, wyr6fx@virginia.edu

Abstract

Concentrated Animal Feeding Operations (CAFOs) pose substantial environmental and public-health risks, while also serving as critical nodes in disease surveillance and climate resilience planning. Yet scalable mapping of CAFOs remains difficult due to heterogeneous data sources, noisy point locations, inconsistent annotations, and systematic under-reporting. We introduce CAFOSat, a strongly annotated, infrastructure-aware dataset for CAFO mapping across the United States. CAFOSat integrates high-resolution NAIP imagery with multi-source, multi-state CAFO location inventories and converts weak publicly available CAFO geo-locations into refined point annotations through a human-in-the-loop pipeline that combines a learned “AI annotator” with GradCAM-based localization and geometric clustering. We further curate hard negative samples using land-cover-guided sampling with spatial exclusion buffers, and provide infrastructure-level labels (e.g., barns, manure ponds, grazing presence) via manual verification. The resulting dataset contains over 45,000 image patches spanning 20 states and four major CAFO. Benchmarking across modern CNN, transformer, and vision-language models demonstrates that refined annotations and curated negatives materially improve performance and generalization. Finally, we introduce a synthetic augmentation pipeline that generates realistic CAFO-like variations to diversify training data, yielding additional gains in robustness under distribution shift. Dataset: <https://huggingface.co/datasets/oishee3003/CAFOSat>, Code: <https://github.com/oishee-hoque/CAFOSat>.

1. Introduction

Concentrated Animal Feeding Operations (CAFOs) are large-scale industrial facilities where substantial numbers

of animals are confined in relatively small areas [1, 2]. The thresholds for classifying an operation as a CAFO vary by livestock type—for example, hundreds of cattle or millions of chickens. With the continued rise in CAFOs across the United States (US), concerns have grown regarding their impact on the environment and public health, particularly within the One Health framework. CAFOs are susceptible to a wide range of infectious diseases that can spill over to humans, and they generate vast quantities of waste, contributing to nutrient runoff, degraded water quality, and air pollution through greenhouse gas emissions [1]. The ongoing Highly Pathogenic Avian Influenza (HPAI) epidemic exemplifies the risks associated with high-density livestock operations [3–6]. Beyond simply identifying CAFO locations, mapping additional attributes such as facility size, livestock type, and structural components—e.g., barns, manure ponds, and storage areas—is critical for accurate risk assessment and epidemiological modeling. CAFOs account for over half of US livestock production, yet their locations and prevalence remain difficult to track due to regulatory gaps and limited transparency [7–9]. Over the years, there have been several efforts from various entities towards identifying CAFO locations (see Handan-Nader et al. [10] for a comprehensive review).

Remote sensing-based methods are popular for mapping and monitoring various agricultural assets at different spatial scales. In the context of livestock, mapping grasslands, livestock operations, and monitoring animals are some examples of problems that have been examined using remote-sensing methods. In recent years, several studies have explored large-scale mapping of CAFOs using remote sensing and machine learning (ML). Deep learning-based methods, in particular, have shown strong potential for accurately identifying CAFO locations over broad spatial extents [2, 10–12]. However, these efforts are often limited in geographic scope, the range of livestock types covered, or both. To support national-scale mapping and to enable estimation of key facility-level attributes, a comprehensive, ML-ready dataset is needed. This requires: (i) aggregating

^{*}Equal contribution.

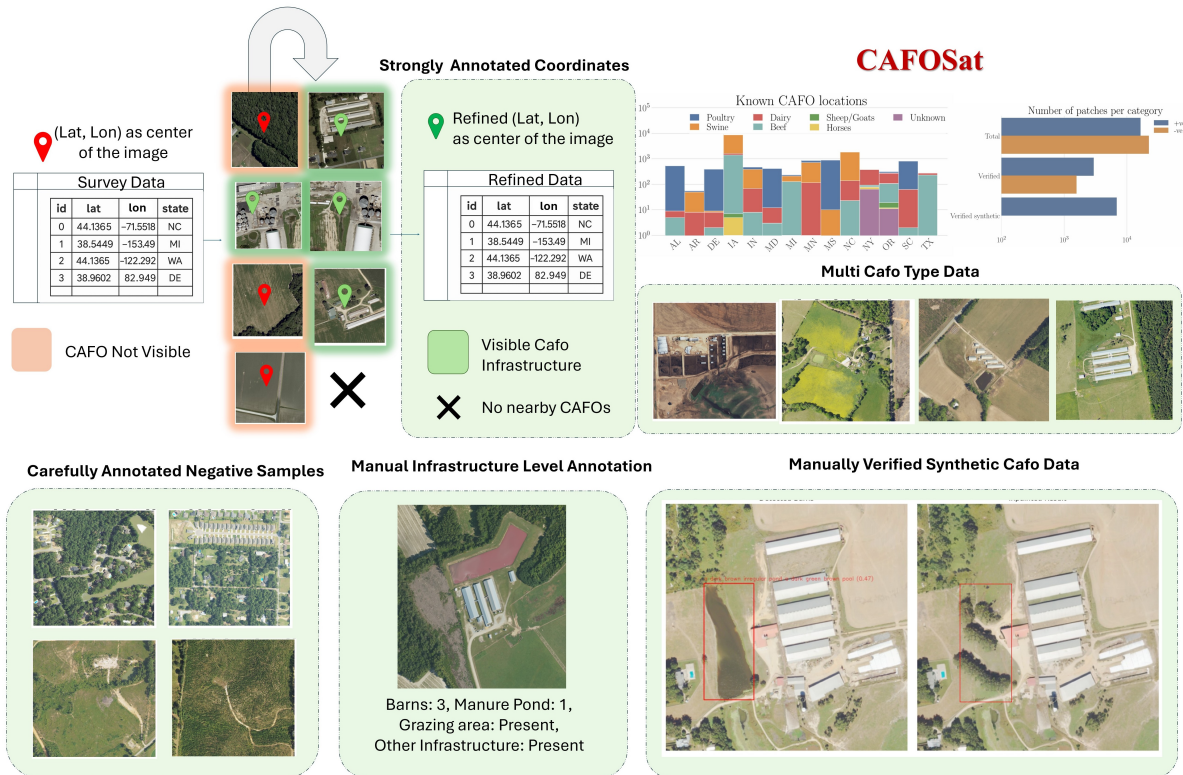


Figure 1. Overview of CAFOSat. (*Top left*) Raw survey coordinates (red pins) serve as initial patch centers; patches with no visible CAFO infrastructure are excluded (×). (*Top center*) The refinement pipeline produces strongly annotated coordinates (green pins) centered on confirmed CAFO infrastructure. (*Top right*) State-wise CAFO location counts by livestock type and patch counts across Total, Verified, and Verified Synthetic subsets; aerial examples illustrate visual diversity across CAFO types. (*Bottom left*) Curated hard-negative samples from non-CAFO land cover. (*Bottom center*) Infrastructure-level annotation recording barn count, manure pond count, grazing area, and other structures. (*Bottom right*) Manually verified synthetic patches with bounding boxes highlighting inpainted infrastructure regions.

all available data on CAFO facility attributes into a high-fidelity database; and (ii) benchmarking established methods, especially in out-of-distribution settings, to reveal key data gaps and modeling challenges.

Challenges. Despite the need for regulation of CAFOs, there is a lack of comprehensive, well-aligned datasets. First, the data has to be assembled from diverse sources (see Table S1) and the coverage is small, spanning a small number of states, resulting in limited geographic diversity and poor generalization to new regions with different facility layouts or land use patterns. The type and amount of information differs widely across these sources. Second, available annotations are often inaccurate or imprecise, typically consisting of point coordinates from regulatory filings that may refer to parcel centroids or access roads rather than the actual facility footprints. Third, under-reporting is common, especially for unpermitted or small-scale operations, introducing systematic false negatives that degrade training quality. Fourth, the visual variability of CAFOs—across animal type, geography, and season—is rarely captured, limiting the representativeness of the training data. Finally, man-

ually refining and validating these locations to align them with imagery is labor-intensive and difficult to scale, posing a bottleneck to creating high-quality training datasets.

Contributions. We address the limitations of current CAFO datasets through a comprehensive framework that combines weak supervision, data refinement, and human-in-the-loop validation to create a *high-quality, large-scale dataset for CAFO detection*. Our approach significantly reduces manual annotation effort while improving label quality. The resulting dataset is diverse, scalable, and supports benchmarking across multiple CAFO types and geographies. Our key contributions are:

- **Benchmark dataset:** We introduce a refined, strongly annotated CAFO dataset spanning 20 U.S. states, containing more than 45,000 NAIP image patches (39,257 base + 6,454 synthetically augmented) at 833×833 pixels with 0.6m spatial resolution, and covering four major CAFO types along with well curated negative samples. The dataset is compiled from several distinct sources, including federal, state, and academic records, ensuring diverse geographic and operational representation. In addition

to facility-level classification, we provide infrastructure-level annotations (e.g., barns, manure ponds) that are manually labeled and verified. It also includes a manually validated synthetic subset, enabling robust evaluation of both real and augmented data. The dataset features both positive samples and a curated set of hard negatives to support comprehensive model training and testing (see Fig. 1).

- **Scalable Annotation Pipeline:** To aid in this process, we develop a generic human-in-the-loop pipeline to refine weakly annotated geolocation data into strongly annotated labels using a scalable, easily extensible framework that significantly reduces manual annotation effort.
- **Comprehensive Evaluation of Annotation Quality:** We demonstrate the utility of our dataset through a series of experiments that highlight the impact of annotation quality and dataset composition on model performance. We also evaluate cross-dataset generalization, training on CAFOSat and testing on external datasets.
- **Reproducibility and Accessibility:** To facilitate adoption and reproducibility, we release all code, data processing scripts, annotation tools, and data loaders as part of a complete pipeline. The accompanying Jupyter notebooks provide ready-to-use examples for training, evaluation, and visualization, lowering the barrier to entry for researchers and practitioners.

2. Related Work

Remote sensing and CAFO Detection: datasets and methods. Robinson et al. [2] demonstrate that deep learning is a promising approach to map poultry operations at scale. They do this by training convolutional neural network (CNN) models on USDA NAIP 1m aerial imagery, using data from portions of four states for training and validation. Hendan et al. [10] apply standard CNNs in their research, but coverage is restricted to swine and poultry operations in North Carolina. Similarly, the Mapping for Environmental Justice (MEJ) [13] dataset is confined to cattle CAFOs in New Mexico and does not include detailed infrastructure labels. METER-ML [11], though broader in geographic scope (comprising four states), targets methane-related facilities and employs multi-resolution imagery (NAIP and Sentinel-2). Chugg et al. [12] target the growth of CAFO facilities over time: they combine state-of-the-art building segmentation with change detection to flag unpermitted barn construction using time-series satellite images by monitoring 1,513 known CAFO sites with Planet’s 3m imagery. A recent work [14] uses a random forest model on publicly available socio-environmental data—not satellite imagery—to map AFOs. Key predictors included canopy cover, land surface temperatures, and phosphorus levels using training data on 18 US states. In contrast, our CAFOSat dataset spans 20 U.S. states and pro-

vides detailed annotations of multiple CAFO types (swine, poultry, cattle, dairy, mixed) along with associated infrastructure, supporting fine-grained and interpretable modeling at national scale (see Table 1).

Weakly Supervised Labeling for inaccurate geolocations. Across the above-mentioned datasets, automated patching may omit key visual elements such as barns, manure ponds, and grazing areas, particularly when facility coordinates are imprecise or resolution is limited. Such omissions can pose challenges for downstream tasks requiring fine-grained infrastructure recognition. Existing CAFO detection works acknowledge this problem. Handan-Nader et al. [10] consider a similar approach as our work based on class-activation maps[15], but only to recenter the predicted infrastructure, followed by manual validation of a subset of predictions. Building on this direction, several studies propose refinements through CAM-based localization and progressive feature learning. Comprehensive reviews [16] outline the broader landscape of weak supervision, highlighting issues related to inexact, incomplete, and inaccurate labels. While these methods provide valuable foundations for learning under spatial uncertainty, these approaches typically assume that the weak labels are still reasonably well aligned. In contrast, our setting involves noisy point annotations that may not even intersect the object of interest, requiring a more robust strategy for localization.

Prompt-Guided Synthetic Image Augmentation in Remote Sensing. Conventional data augmentation in remote sensing—such as geometric or spectral transformations [17]—does not capture the semantic complexity needed for fine-grained tasks like CAFO infrastructure analysis. To improve data diversity and address class imbalance, recent work has explored using generative models and vision-language prompts to synthetically expand underrepresented classes [18, 19]. Vision-language models (e.g., GroundingDINO [20]) enable open-vocabulary object detection via natural language, while diffusion-based inpainting [21] supports realistic structure editing. Moreover, DiffusionSat [22] and GeoSynth [23] demonstrate that diffusion models can generate high-resolution satellite imagery conditioned on text, metadata, and spatial context, while more task-specific studies have explored prompt-driven augmentation for Earth observation datasets [24] and synthetic generation for rare objects [25]. These works motivate the use of generative models in remote sensing, but our goal differs: rather than generating fully synthetic scenes, we apply targeted, infrastructure-aware inpainting to create label-preserving CAFO variations that increase structural diversity while maintaining semantic validity.

3. Data Processing Pipeline

A detailed description of all data sources used to construct CAFOSat, including satellite imagery, CAFO location in-

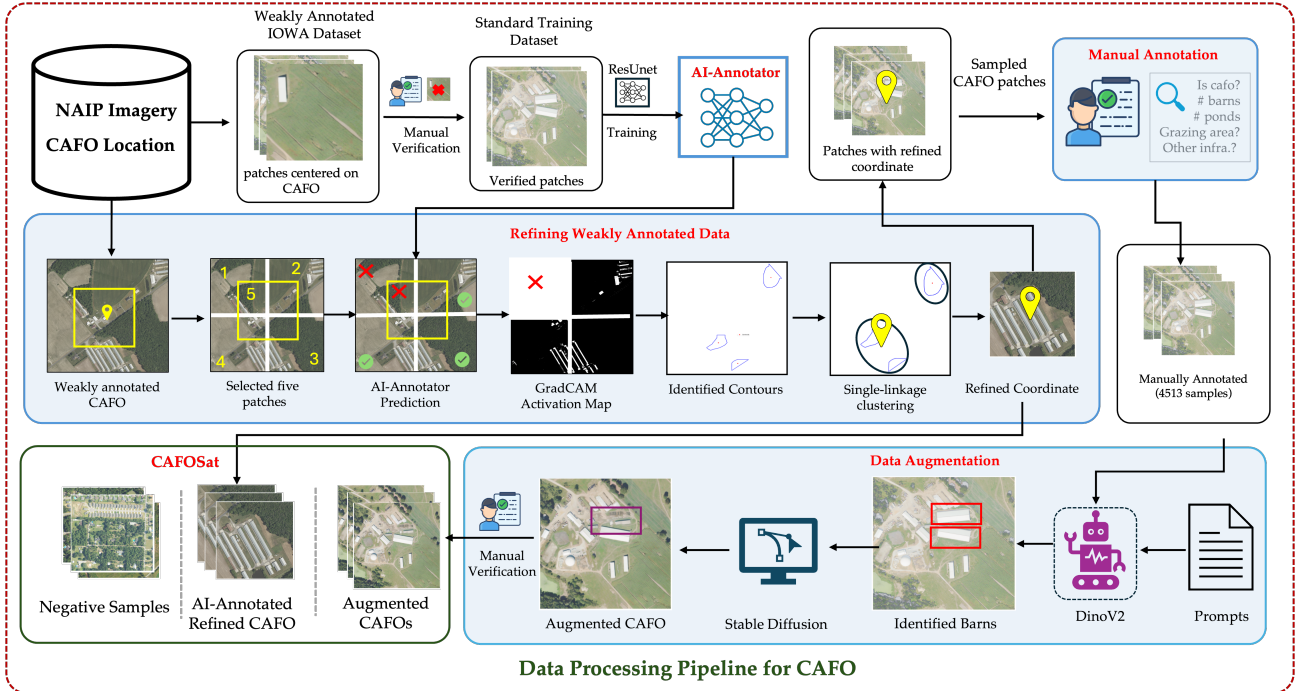


Figure 2. Data processing pipeline for CAFOSat. (Top) An AI-Annotator trained on verified patches is used to pre-filter CAFO candidates for manual annotation. (Middle) Weakly annotated locations are refined via five overlapping patch extractions, GradCAM activation mapping, contour extraction, and single-linkage clustering to produce spatially accurate coordinates; 4,513 samples are then manually verified with infrastructure-level annotations (e.g., barn counts, manure ponds, grazing areas). (Bottom right) A prompt-guided augmentation pipeline uses text prompts and DINOv2 to identify infrastructure (e.g., barns), which is subsequently inpainted using Stable Diffusion and manually verified. (Bottom left) The final CAFOSat dataset comprises three components: carefully curated negative samples, AI-annotated refined CAFO patches, and manually verified synthetic augmented patches, all accompanied by manually annotated infrastructure-level information.

Table 1. Comparison of existing ML-ready datasets for CAFO identification.

Dataset	Coverage	CAFO Types	Infrastructure	# CAFOs
METER-ML [11]	NC, MI, CA, MN	✗	✗	6,979
RegLab [10]	North Carolina	Swine/Poultry	✗	4,984
MEJ-Dataset [13]	New Mexico	Cattle	✗	160
CAFOSat (Ours)	20 U.S. states	Swine/Poultry/Cattle/Dairy/Mixed	Barn, Pond, Grazing	18,441

ventories, and land use masks, is provided in the supplementary material (Section B).

CAFOSat Overview. The pipeline produces CAFOSat, a dataset of $\sim 45,000$ NAIP image patches (833×833 px, 0.6 m resolution) spanning 20 U.S. states, plus 20,771 curated negatives. The full release covers six livestock categories (Swine, Poultry, Dairy, Beef, Horses, Sheep/Goats); benchmarking experiments use the four major types (Swine, Poultry, Dairy, Beef) alongside the Negative class, as Horses and Sheep/Goats are excluded due to insufficient sample sizes (24 and 21 samples respectively). Each sample includes: (i) a facility-level classification label (Swine, Poultry, Dairy, Beef, Horses, Sheep/Goats, or Negative);

(ii) infrastructure-level annotations (barn count, manure pond count, grazing area and other structure presence) for 4,513 manually verified patches (Table 2); (iii) geospatial metadata including original and refined coordinates, bounding boxes, and state; (iv) augmentation metadata for 6,454 synthetic patches; and (v) six pre-defined train/val/test splits for reproducible benchmarking. The dataset, data loaders, and processing scripts are publicly available. Full details of all provided fields and split configurations are described in the supplement (Section A).

An overview of the data processing pipeline is provided in Figure 2. We follow five steps to generate CAFOSat:

Standardized Training Data Creation. To construct

Table 2. CAFOSat dataset composition by category and split, with infrastructure-level annotation counts. The `Verified-Set` is verified benchmark spanning states unseen during training; the `Held-Out Set` is the in-distribution holdout evaluation set. Infrastructure counts reflect manually annotated positive samples in the full dataset. Horses, Sheep/Goats, and Other/Unknown categories are retained in the released dataset but excluded from benchmarking due to insufficient or ambiguous sample sizes. [†]Full dataset (39,212) + synthetically augmented samples (6,454) \approx 45,000 total patches reported in the abstract.

Category	Split Counts				Infrastructure Annotations			
	Train	Verified-Set	Held-Out Set	Total [†]	Barn	Manure Pond	Grazing Area	Other Infra.
Negative	14,954	1,570	3,116	20,771	—	—	—	—
Swine	6,330	972	1,320	11,220	1,150	548	400	889
Poultry	1,546	1,239	326	3,576	1,033	298	528	458
Dairy	484	405	100	1,643	359	182	135	250
Beef	1,092	281	232	2,002	257	101	94	207
Total	24,406	4,467	5,094	39,212	2,799	1,129	1,157	1,804

a high-quality training dataset, we start by selecting all CAFOs from the CAFOMaps [26] dataset, which has a diverse set of livestock operations (e.g., poultry, beef, dairy, and swine) to ensure sufficient sample diversity. We follow standard remote sensing practices by first geo-locating all 4513 verified CAFO coordinates and mapping them to the corresponding NAIP satellite imagery. For each location, we extract a fixed-size 833×833 pixel patch centered on the CAFO. The patch dimensions are carefully selected based on domain knowledge (i.e., CAFO infrastructure can span up to 1,000–1,500 meters in length), ensuring that the full extent of facilities such as barns, manure lagoons, and feedlots is captured. All generated patches are then manually verified and annotated using binary labels (CAFO or non-CAFO).

AI Annotator. To construct our initial *Standard Training Set*, we begin with labeled CAFO samples from RegLab [10], which includes a small number of manually verified poultry and swine facilities. Using this data, we train a ResNet-based binary classification model, which we then employ as an AI annotator to identify likely CAFO patches from our collected CAFOMaps [26] dataset — selected for its broader diversity of CAFO types. To reduce manual effort and improve efficiency, we use the AI annotator to pre-filter candidate patches, focusing only on those where the model predicts CAFO presence with high confidence (softmax probability ≥ 0.8). This strategy significantly narrows the verification workload while maintaining label quality. The model is applied specifically to poultry and swine patches, and all 3,286 positively predicted samples (1,615 Swine + 1,671 Poultry) are manually verified to ensure high label quality. This verification is essential, as the original location data is noisy, and our goal is to build a small, strongly annotated training set. To further increase class diversity, we manually verify all dairy and beef patches, obtaining an additional 383 dairy and 209 beef CAFO samples. These verified samples, combined with

carefully curated negative examples, comprise our *Standard Training Set*, which is used throughout the rest of our experiments. Note that while the Iowa data is used for candidate selection and verification, it is excluded from training due to its differing image resolution.

Refining Weakly Annotated Data. Given that CAFO location annotations are often weak, we propose a refinement algorithm that transforms these coarse coordinates into spatially accurate point annotations using model-guided attention (GradCAM) and geometric clustering. Our process is shown in Algorithm 1. Starting from a weak coordinate annotation c_{center} , we extract five patches of shape 833×833 pixels: one centered at c_{center} and four diagonally offset by 416 pixels to ensure local spatial coverage. Each patch is evaluated using the AI annotator created in the previous step. Patches predicted as CAFOs are then processed with GradCAM to generate class-specific attention heatmaps. These heatmaps are thresholded at level τ to isolate high-confidence activation regions, which are converted into polygonal shapes via connected-component analysis. GradCAM heatmaps are computed using the *torchcam* library [27]. To localize the dominant CAFO structure, we apply single-linkage clustering to the extracted polygons using a minimum inter-polygon distance threshold d_{merge} , which groups spatially contiguous regions that likely correspond to a single CAFO. The final refined coordinate is computed as the centroid of the merged polygon from the largest cluster (based on polygon counts). Patches associated with smaller clusters are discarded, as they likely correspond to spurious activations or unrelated structures rather than the primary CAFO facility.

Manual Verification & Annotation. To assess annotation quality, we manually verified a total of 4,513 samples. The `Verified` set was constructed using a stratified sampling strategy: we included all 2,344 samples labeled as negative by the AI annotator, and additionally sampled 2,169 instances uniformly at random from the remaining pool. For

Algorithm 1: CAFO Coordinate Refinement via Classification and GradCAM Clustering

Input: Image I ; center coordinate $c_{\text{center}} \in \mathbb{R}^2$; classifier \mathcal{A} ;
GradCAM threshold τ ; clustering distance d_{merge}

Output: Refined coordinate $c^* \in \mathbb{R}^2$

```
 $r \leftarrow 416$  ;  
 $c_0 \leftarrow c_{\text{center}}$  ;  
 $c_1 \leftarrow c_0 + (r, r)$ ,  $c_2 \leftarrow c_0 + (r, -r)$ ,  $c_3 \leftarrow c_0 + (-r, r)$ ,  
 $c_4 \leftarrow c_0 + (-r, -r)$  ;  
Extract patches  $P_i$  of size  $833 \times 833$  pixels centered at  $c_i$  for  
 $i = 0, \dots, 4$  ;  
 $\mathcal{P}_{\text{CAFO}} \leftarrow \{P_i \mid \mathcal{A}(P_i) = 1\}$  ;  
 $\mathcal{G} \leftarrow \emptyset$  ;  
foreach  $P \in \mathcal{P}_{\text{CAFO}}$  do  
     $H \leftarrow \text{GradCAM}(P)$  ;  
     $M \leftarrow \{(x, y) \mid H(x, y) \geq \tau\}$  ;  
    Extract connected components  $\{R_k\}$  from  $M$  ;  
    Convert each  $R_k$  to minimum bounding polygon  $G_k$  and  
    update  $\mathcal{G} \leftarrow \mathcal{G} \cup \{G_k\}$  ;  
Perform single-linkage clustering on  $\mathcal{G}$  :  
     $\text{dist}(G_i, G_j) = \min_{x \in G_i, y \in G_j} \|x - y\|_2$  ;  
Let  $\mathcal{G}^* \subseteq \mathcal{G}$  be the largest resulting cluster ;  
 $G_{\text{merged}} \leftarrow \bigcup \mathcal{G}^*$  ;  
 $c^* \leftarrow \text{Centroid}(G_{\text{merged}})$  ;  
return  $c^*$  ;
```

each CAFO patch, we provide infrastructure-level annotations: we manually count the number of visible barns and manure ponds, and record the presence or absence of grazing areas and other non-barn structures.

Negative Sample Generation. We employ a stratified negative sampling strategy guided by land use data to generate non-CAFO training samples. Specifically, we use 30-meter resolution land cover maps to identify land types where CAFOs are plausibly located. Across all studied states, we select eight relevant land use classes: pasture, grassland, developed, semi-developed, cropland, barren land, shrubland, and open space/water. From each land use category, we randomly sample 3,000 candidate coordinates, resulting in a diverse pool of negative samples stratified by land cover type. To ensure that sampled points do not overlap with nearby CAFO infrastructures, we apply a 1.5-kilometer exclusion radius around all known CAFO locations (any candidate point within this buffer was discarded). The remaining coordinates are used to extract fixed-size image patches (833×833 pixels) centered on each location, ensuring all patches fall within valid image bounds. This process yields a total of 20,771 high-confidence negative samples for robust classifier training.

Prompt-Guided Data Augmentation. To improve model generalization in CAFO infrastructure analysis, we develop a prompt-guided augmentation pipeline that removes visually identifiable structures, such as barns, manure ponds, and other supporting facilities, and replaces them with semantically plausible non-infrastructure content. This results in label-preserving image variants that diversify struc-

tural configurations while retaining the associated CAFO types (e.g., swine, dairy, poultry) as defined in the metadata. In total, 6,454 unique patches were augmented; individual patches may contain multiple infrastructure types, yielding 3,921 barn, 1,344 manure pond, and 2,089 other infrastructure removal operations across the augmented set (see Figure S1 in Supplement).

First, we perform **infrastructure detection via vision-language prompts**, where the objective is to localize and identify physical structures within satellite imagery. Using GroundingDINO [20], a vision-language object detector, we detect infrastructure based on natural language prompts that encode high-level visual priors observed in overhead imagery. We carefully designed 25 prompts that capture structural characteristics of CAFOs across livestock types; details are in the supplement. The second part is **inpainting for structure removal**, where we generate binary masks from subsets of predicted bounding boxes (up to five per image) and use these to guide the removal of detected infrastructure. The RGB image and corresponding mask are passed to a Stable Diffusion Inpainting model [28], conditioned on non-infrastructure prompts (e.g., “grassland”, “a small water pool”, “cluster of trees”). The model synthesizes contextually consistent content to fill the masked regions. To preserve the validity of the CAFO type label, we remove infrastructure only when multiple instances are present within a patch — for example, if ten barns are detected, a subset (e.g., two or three) are removed to ensure the structural identity of the facility remains intact. This process generates the *Augmented Set*. Detailed metadata is provided for each sample to ensure full traceability and label integrity across all synthetically generated patches.

Our prompt-guided augmentation strategy builds on a growing body of work applying generative models to expand remote sensing training data. Conventional augmentation approaches such as geometric and spectral transformations [17] do not capture the semantic variability needed for fine-grained infrastructure recognition. Recent work has explored diffusion-based inpainting and vision-language guidance to synthesize semantically consistent remote sensing imagery [18, 19], including satellite-image-specific generative models such as DiffusionSat [22] and GeoSynth [23]. Our approach extends this direction to agricultural infrastructure, using GroundingDINO for open-vocabulary localization and Stable Diffusion for structure-aware inpainting, while preserving CAFO type labels through a multi-instance removal constraint.

4. Analysis and Benchmarking

We evaluate CAFOSat along four dimensions: (i) the effect of annotation refinement on classification performance, (ii) cross-dataset transfer between CAFOSat and prior CAFO datasets, (iii) multiclass benchmark performance on two

Table 3. Performance comparison of different models on two evaluation sets. The *Verified-Set* (4,513 samples) spans out-of-distribution states unseen during training; the *Held-Out Set* (5,103 samples) is an in-distribution random holdout. F1 and mAP are macro-averaged. Per-class F1 scores are reported for the four major CAFO types.

Model	Verified-Set							Held-Out Set						
	Acc.	F1	mAP	Swine	Poultry	Dairy	Beef	Acc.	F1	mAP	Swine	Poultry	Dairy	Beef
ResNet18	0.596	0.383	0.401	0.579	0.838	0.405	0.574	0.939	0.481	0.511	0.930	0.851	0.391	0.695
ResNet50	0.601	0.399	0.444	0.578	0.819	0.591	0.608	0.935	0.482	0.513	0.923	0.830	0.505	0.613
ViT-B/16	0.596	0.377	0.374	0.581	0.826	0.545	0.437	0.934	0.492	0.528	0.919	0.859	0.569	0.609
Swin-B	0.630	0.421	0.443	0.600	0.853	0.655	0.655	0.952	0.527	0.559	0.946	0.873	0.670	0.736
ConvNeXt	0.626	0.400	0.412	0.592	0.852	0.626	0.633	0.945	0.544	0.593	0.938	0.861	0.622	0.691
EfficientNet	0.636	0.405	0.431	0.599	0.867	0.634	0.640	0.949	0.517	0.547	0.946	0.890	0.581	0.729
CLIP	0.492	0.292	0.298	0.503	0.675	0.441	0.308	0.878	0.415	0.420	0.855	0.706	0.352	0.445
RemoteCLIP	0.560	0.317	0.342	0.544	0.767	0.461	0.327	0.912	0.453	0.486	0.898	0.764	0.488	0.497
DINOv2	0.602	0.364	0.371	0.569	0.835	0.524	0.530	0.921	0.469	0.483	0.910	0.811	0.468	0.587

standardized CAFOSat evaluation splits, and (iv) the impact of synthetic augmentation on model robustness.

Evaluation Sets. We define two complementary evaluation sets. (i) **Verified-Set:** 4,513 manually verified samples, including unseen states during training (AR, CA, FL, GA), providing a controlled benchmark for geographic generalization. (ii) **Held-Out Set:** 5,103 samples held out from in-distribution states, serving as a standard random holdout evaluation. Model details and metrics are provided in the supplement.

Impact of Annotation Quality on Performance. We study whether improving coordinate alignment (via manual refinement) increases CAFO classification performance. We train binary classifiers on three sources—RegLab [10], METER-ML [11], and our *Standard Training Set* (Sec. 3)—and evaluate on CAFOSat CAFO-only patches extracted using either the original (survey-reported) coordinates or the refined coordinates. We restrict this evaluation to CAFO patches because refinement is applied to known CAFO locations; a well-centered patch should contain visible CAFO infrastructure and thus be classified as CAFO. Table 4 compares performance on weak vs. refined patch extractions. Across models, refined patches consistently yield higher accuracy, indicating that better spatial alignment increases the visibility of discriminative CAFO structures and improves recognition.

We further assess cross-dataset generalization to position CAFOSat as both a training resource and a benchmark. Table 5 reports models trained on METER-ML and RegLab and evaluated on the full CAFOSat dataset (CAFO and non-CAFO). METER-ML trained models transfer reasonably well, whereas RegLab trained models transfer is weaker, highlighting domain gaps (i.e., state-wise variation) and the need for representative supervision. Conversely, Table 6 shows that models trained on CAFOSat generalize well to the *Verified-Set*, METER-ML, and RegLab; transformer-based models (e.g., ViT-B/16) achieve strong accuracy and F1 on the *Verified-Set*. Overall, these re-

sults demonstrate that CAFOSat provides high-quality supervision, benefits from refined annotations, and supports robust cross-dataset evaluation.

Benchmarking. To benchmark the effectiveness of deep learning models for multiclass CAFO classification, we evaluated a suite of nine diverse architectures: ResNet18/50 [29], EfficientNet [30], ConvNeXt [31], ViT-B/16 [32], Swin-B [33], DINOv2 [34], CLIP [35], and RemoteCLIP [36]. These models span a range of design paradigms—from classical CNNs to self-attention-based transformers and multimodal pretrained systems—providing a comprehensive view of current capabilities. All models were trained on our curated CAFO dataset and assessed across two standardized evaluation sets: (i) *Verified-Set* and (ii) *Held-Out Set*. The results in Table 3 show that transformer-based models (e.g., Swin-B and EfficientNet) generally outperform CNN-based baselines such as ResNet, with notably stronger per-class F1 and mean Average Precision (mAP). Across both sets, Poultry is the easiest class to recognize while Dairy is the hardest, due to visual similarity with Beef CAFO structures. More results are reported in Table S3 and Figure S3 in the supplementary material.

Effectiveness of Synthetic Augmentation. To quantify how much synthetic CAFO imagery can substitute for, and complement, real annotations during training, we compare models trained on real-only (samples from *Verified-set*) and synthetic-only (samples from *Augmented dataset*). Note that each training set included 20% negative samples from CAFOSat for class balance. We select best performing vision transformer model (Swin-B) and convolutional model (ConvNeXt)—top-performing models from prior benchmarking. As shown in Table 7, we notice that model trained on augmented dataset produce similar performance (with a drop of only 0.6% F1 and 2.2% mAP) as model trained on verified annotated dataset. It is worth noting that performance gap for transformer based model are lower than CNN based model. These results under-

Table 4. Impact of annotation quality on CAFO detection performance. Binary classifiers are trained on three source datasets (RegLab, METER-ML, and our Standard Training Set) and evaluated on CAFOSat CAFO-only patches extracted using either weakly annotated (Weak.) survey coordinates or spatially refined (Ref.) coordinates. Higher scores indicate better recognition of visible CAFO infrastructure.

Train Dataset	ResNet18		ResNet50		ViT-B/16		Swin-B	
	Weak.	Ref.	Weak.	Ref.	Weak.	Ref.	Weak.	Ref.
RegLab [10]	0.357	0.375	0.070	0.071	0.552	0.601	0.521	0.547
METER-ML [11]	0.595	0.659	0.441	0.507	0.718	0.766	0.638	0.660
<i>Standard Training Set</i>	0.767	0.883	0.870	0.931	0.791	0.894	0.891	0.979

Table 5. Evaluating external dataset generalization on the CAFOSat benchmark. Models trained on METER-ML or RegLab are evaluated on the full CAFOSat dataset (binary CAFO vs. non-CAFO).

Train Dataset	Model	Acc.	F1	CAFO Acc.
METER-ML [11]	Swin-B	0.823	0.809	0.659
	ViT-B/16	0.869	0.862	0.766
RegLab [10]	Swin-B	0.739	0.686	0.394
	ViT-B/16	0.786	0.768	0.601

Table 6. Benchmarking CAFOSat-trained models on the Verified-Set and external datasets for binary CAFO vs Non-CAFO classification. R denotes macro recall; CAFO Acc. is accuracy on positive CAFO samples only.

Test Dataset	Model	Acc.	F1	R	CAFO Acc.
Verified-Set	ResNet18	0.714	0.631	0.627	0.911
	ResNet50	0.701	0.609	0.610	0.911
	ViT-B/16	0.928	0.925	0.921	0.878
	Swin-B	0.702	0.614	0.614	0.902
METER-ML [11]	ResNet18	0.831	0.817	0.808	0.658
	ResNet50	0.849	0.836	0.825	0.676
	ViT-B/16	0.761	0.719	0.718	0.441
	Swin-B	0.810	0.788	0.779	0.580
RegLab [10]	ResNet18	0.944	0.822	0.777	0.567
	ResNet50	0.946	0.813	0.750	0.504
	ViT-B/16	0.914	0.619	0.582	0.165
	Swin-B	0.966	0.903	0.880	0.772

Table 7. Performance across two training setups evaluated on the Held-Out Set. *Annotated*: manually verified samples only; *Augmented*: synthetic inpainted samples only.

Model	Type	F1	mAP
<i>Swin-B</i>	Annotated	0.770	0.495
	Augmented	0.764 (0.6%↓)	0.473 (2.2%↓)
<i>ConvNeXt</i>	Annotated	0.835	0.500
	Augmented	0.799 (3.6%↓)	0.480 (2.0%↓)

score the complementary value of augmentation, particularly for transformer-based models in data-scarce or imbal-

anced contexts.

5. Conclusion

CAFOSat addresses a key obstacle in scalable CAFO mapping: public inventories exist at scale, but their geolocations are often noisy, and this misalignment substantially degrades learning from overhead imagery. Our results show that refining weak point labels is a first-order driver of performance, often rivaling the effect of changing model families, by re-centering patches on the visually salient infrastructure. Across architectures, transformer-based and pretrained models generally achieve the best overall accuracy—especially in CAFO recall and mAP—suggesting that global context and layout cues are critical for distinguishing CAFOs from visually similar agricultural facilities. We also find that synthetic augmentation can improve robustness by diversifying the training distribution, though benefits are not uniform, motivating adaptive filtering/weighting of synthetic samples. Limitations include incomplete geographic coverage and potential reporting biases in source inventories, residual confusion with hard negatives, and the simplifications inherent to patch-based classification; future work should extend CAFOSat toward detection/segmentation, temporal modeling, and uncertainty-aware screening for large-area monitoring. CAFOSat inherits biases from public inventories, imagery, and annotation procedures, leading to potential regional coverage gaps, outdated records, and uneven label quality. Additionally, its U.S.-centric scope and underrepresentation of rare facility configurations may limit generalization to other geographies and atypical infrastructure layouts. Moreover, publicly available ML-ready geospatial datasets and regulatory definitions are often less standardized internationally, limiting direct comparison across countries. In future, we will work on foundation for extending infrastructure-aware live-stock mapping to broader international settings.

Acknowledgment

This material is based upon work supported by the AI Research Institutes program supported by NSF and USDA-NIFA under the AI Institute: Agricultural AI for Transforming Workforce and Decision Support (AgAID) award

No. 2021-67021-35344. This work was partially supported by University of Virginia Strategic Investment Fund award number SIF160.

References

- [1] A. Moses and P. Tomaselli, "Industrial animal agriculture in the united states: Concentrated animal feeding operations (cafos)," *International farm animal, wildlife and food safety law*, pp. 185–214, 2017. 1
- [2] C. Robinson, B. Chugg, B. Anderson, J. M. L. Ferres, and D. E. Ho, "Mapping industrial poultry operations at scale with deep learning and aerial imagery," *IEEE Journal of Selected Topics in Applied Earth Observations and Remote Sensing*, vol. 15, pp. 7458–7471, 2022. 1, 3
- [3] D. J. Prosser, C. M. Kent, J. D. Sullivan, K. A. Patyk, M.-J. McCool, M. K. Torchetti, K. Lantz, and J. M. Mullinax, "Using an adaptive modeling framework to identify avian influenza spillover risk at the wild-domestic interface," *Scientific Reports*, vol. 14, no. 1, p. 14199, 2024. 1
- [4] J. M. Humphreys, A. M. Ramey, D. C. Douglas, J. M. Mullinax, C. Soos, P. Link, P. Walther, and D. J. Prosser, "Waterfowl occurrence and residence time as indicators of h5 and h7 avian influenza in north american poultry," *Scientific Reports*, vol. 10, no. 1, p. 2592, 2020.
- [5] A. Adiga, A. Chopra, M. L. Wilson, S. Ravi, D. Xie, S. Swarup, B. Lewis, R. Raskar, and M. V. Marathe, "A high-resolution, us-scale digital similar of interacting livestock, wild birds, and human ecosystems with applications to multi-host epidemic spread," *arXiv preprint arXiv:2411.01386*, 2024.
- [6] T.-Q. Nguyen, C. R. Hutter, A. Markin, M. Thomas, K. Lantz, M. L. Killian, G. M. Janzen, S. Vijendran, S. Wagle, B. Inderski *et al.*, "Emergence and interstate spread of highly pathogenic avian influenza a (h5n1) in dairy cattle in the united states," *Science*, vol. 388, no. 6745, p. eadq0900, 2025. 1
- [7] D. Gurian-Sherman, *CAFOs Uncovered: The Untold Costs of Confined Animal Feeding Operations*. Union of Concerned Scientists, 2008. 1
- [8] C. Hribar, "Understanding Concentrated Animal Feeding Operations and Their Impact on Communities," National Association of Local Boards of Health, Tech. Rep., 2010.
- [9] C. Handan-Nader, D. E. Ho, and L. Y. Liu, "Deep Learning with Satellite Imagery to Enhance Environmental Enforcement," in *Data Science Applied to Sustainability Analysis*. Elsevier, 2021, pp. 205–228. 1
- [10] C. Handan-Nader and D. E. Ho, "Deep learning to map concentrated animal feeding operations," *Nature Sustainability*, vol. 2, no. 4, pp. 298–306, 2019. 1, 3, 4, 5, 7, 8
- [11] B. Zhu, N. Lui, J. Irvin, J. Le, S. Tadwalkar, C. Wang, Z. Ouyang, F. Y. Liu, A. Y. Ng, and R. B. Jackson, "Meter-ml: a multi-sensor earth observation benchmark for automated methane source mapping," *arXiv preprint arXiv:2207.11166*, 2022. 3, 4, 7, 8
- [12] B. Chugg, B. Anderson, S. Eicher, S. Lee, and D. E. Ho, "Enhancing environmental enforcement with near-real-time monitoring: Likelihood-based detection of structural expansion of intensive livestock farms," *International Journal of Applied Earth Observation and Geoinformation*, vol. 103, p. 102463, 2021. [Online]. Available: <https://www.sciencedirect.com/science/article/pii/S0303243421001707> 1, 3
- [13] V. Ehrenpreis, M. Worsham, N. Clarke, and A. Buchholz, "Using machine learning to map concentrated animal feeding operations in new mexico," Mapping for Environmental Justice, Tech. Rep., January 2021, report prepared for the McGovern Foundation. [Online]. Available: <https://mappingforej.studentorg.berkeley.edu/wp-content/uploads/2022/03/NM-CAFO-Report.pdf> 3, 4
- [14] A. Saha, B. Rashid, T. Liu, L. Miralha, and R. L. Muenich, "Machine learning-based identification of animal feeding operations in the united states on a parcel-scale," *Science of The Total Environment*, vol. 960, p. 178312, 2025. 3
- [15] R. R. Selvaraju, M. Cogswell, A. Das, R. Vedantam, D. Parikh, and D. Batra, "Grad-cam: Visual explanations from deep networks via gradient-based localization," in *Proceedings of the IEEE International Conference on Computer Vision (ICCV)*, 2017, pp. 618–626. 3
- [16] X. Li, Z. Tang, G.-S. Xia, and L. Zhang, "Optical remote sensing image understanding with weak supervision: A comprehensive review," *arXiv preprint arXiv:2204.09120*, 2022. 3
- [17] X. Zhu, D. Tuia, L. Mou, G.-S. Xia, L. Zhang, F. Xu, and F. Fraundorfer, "Deep learning in remote sensing: A comprehensive review and list of resources," *IEEE Geoscience and Remote Sensing Magazine*, vol. 5, no. 4, pp. 8–36, 2017. 3, 6
- [18] T. Chen, X. Li, K. Sohn, Z. Wang, L. Yuan, and H. Zhang, "Diffusion-aug: Unlocking the power of diffusion models for visual recognition," *arXiv preprint arXiv:2302.07685*, 2023. 3, 6
- [19] Y. Wang, H. Tan, and H. Yu, "Prompdiffusion: Generating large-scale datasets with subject-prompt alignment," *arXiv preprint arXiv:2308.07974*, 2023. 3, 6
- [20] S. Liu, F. Li, H. Wu *et al.*, "Grounding dino: Marrying dino with grounded pre-training for open-set object detection," *arXiv preprint arXiv:2303.05499*, 2023. 3, 6
- [21] R. Rombach, A. Blattmann, D. Lorenz, P. Esser, and B. Ommer, "High-resolution image synthesis with latent diffusion models," in *Proceedings of the IEEE/CVF Conference on Computer Vision and Pattern Recognition*, 2022, pp. 10 684–10 695. 3
- [22] S. Khanna, P. Liu, L. Zhou, C. Meng, R. Rombach, M. Burke, D. Lobell, and S. Ermon, "Diffusionsat: A generative foundation model for satellite imagery," *arXiv preprint arXiv:2312.03606*, 2023. 3, 6
- [23] S. Sastry, S. Khanal, A. Dhakal, and N. Jacobs, "Geosynth: Contextually-aware high-resolution satellite image synthesis," in *Proceedings of the IEEE/CVF Conference on Computer Vision and Pattern Recognition*, 2024, pp. 460–470. 3, 6
- [24] T. A. DE JESUS SOUSA, B. RIES, and N. GUELF, "Data augmentation in earth observation: A diffusion model approach," 2024. 3

- [25] T. V. Nguyen, J. Hoster, A. Glaser, K. Hildebrand, and F. Biessmann, "Generating synthetic satellite imagery for rare objects: An empirical comparison of models and metrics," *arXiv preprint arXiv:2409.01138*, 2024. 3
- [26] Department of Geographical and Sustainability Sciences, University of Iowa, "Cafomaps: Concentrated animal feeding operations in the united states," <https://www.cafomaps.org/>, 2025, accessed: 2025-05-16. 5, 2
- [27] F.-G. Fernandez, "TorchCAM: Class activation explorer," <https://github.com/frgfm/torch-cam>, March 2020. 5
- [28] R. Rombach, A. Blattmann, D. Lorenz, P. Esser, and B. Ommer, "High-resolution image synthesis with latent diffusion models," in *Proceedings of the IEEE/CVF Conference on Computer Vision and Pattern Recognition (CVPR)*, June 2022, pp. 10 684–10 695. 6
- [29] K. He, X. Zhang, S. Ren, and J. Sun, "Deep residual learning for image recognition," *CVPR*, 2016. 7
- [30] M. Tan and Q. Le, "Efficientnet: Rethinking model scaling for convolutional neural networks," *ICML*, 2019. 7
- [31] Z. Liu, H. Mao, C.-Y. Wu, C. Feichtenhofer, T. Darrell, and S. Xie, "A convnet for the 2020s," *CVPR*, 2022. 7
- [32] A. Dosovitskiy, L. Beyer, A. Kolesnikov, D. Weissenborn, X. Zhai, T. Unterthiner, M. Dehghani, M. Minderer, G. Heigold, S. Gelly, J. Uszkoreit, and N. Houlsby, "An image is worth 16x16 words: Transformers for image recognition at scale," *ICLR*, 2021. 7
- [33] Z. Liu, Y. Lin, Y. Cao, H. Hu, Y. Wei, Z. Zhang, S. Lin, and B. Guo, "Swin transformer: Hierarchical vision transformer using shifted windows," *ICCV*, 2021. 7
- [34] M. Oquab, T. Darcet, T. Moutakanni, A. Ramé, D. Haziza, J. Suárez, M. Szafraniec, Y. Kalantidis, Y. Elkabetz, M. Cord *et al.*, "Dinov2: Learning robust visual features without supervision," *arXiv preprint arXiv:2304.07193*, 2023. 7
- [35] A. Radford, J. W. Kim, C. Hallacy, A. Ramesh, G. Goh, S. Agarwal, G. Sastry, A. Askell, P. Mishkin, J. Clark *et al.*, "Learning transferable visual models from natural language supervision," *ICML*, 2021. 7
- [36] A. Mallya, G. Chen, W. Xie, X. Zhu, D. Lobell, and S. Ermon, "Learning from noisy remote sensing data with vision-language models," in *NeurIPS*, 2022. 7
- [37] U.S. Department of Agriculture, "National Agriculture Imagery Program (NAIP)," <https://www.fsa.usda.gov/programs-and-services/aerial-photography/imagery-programs/naip-imagery/>, 2023, <https://www.fsa.usda.gov/programs-and-services/aerial-photography/imagery-programs/naip-imagery/>. 2
- [38] IndianaMap, "Confined feeding operations - indianamap," <https://www.indianamap.org/datasets/INMap::confined-feeding-operations/about>, 2024, accessed: 2024-05-15. 2
- [39] I. G. Portal, "Iowa animal feeding operations gis data," <https://geodata.iowa.gov/documents/abfbd972640d4e87b6c48dc669775767/about>, 2024, accessed: 2024-05-15.
- [40] M. D. of the Environment, "Animal feeding operations map," <https://catalog.data.gov/dataset/maryland-department-of-the-environment-lma-resource-management-program-animal-feeding-oper-5fb42>, 2024, accessed: 2024-05-15.
- [41] Michigan EGLE GIS Hub, "Cafo locations - michigan department of environment, great lakes, and energy," <https://gis-egle.hub.arcgis.com/datasets/f0843875e5874d04b06396de8200cf75/explore?location=43.005451%2C-83.963570%2C6.10>, 2024, accessed: 2024-05-15.
- [42] M. G. Commons, "Minnesota cafo locations (layer 0)," <https://www.arcgis.com/home/item.html?id=6d119156229d4e908e22f027bd4ee6be&sublayer=0>, 2024, accessed: 2024-05-15.
- [43] New York Department of State, "New york cafo dataset," <https://opdgis.dos.ny.gov/datasets/a9a8eae80864ab98680899ecdbc1c50/explore?location=42.664852%2C-76.586900%2C7.22>, 2024, accessed: 2024-05-15.
- [44] D. D. of Natural Resources, "Delaware cafo map viewer," <https://experience.arcgis.com/experience/c6749f8b31d143cbb38a26fc1b89a2be/page/Delaware>, 2024, accessed: 2024-05-15. 2
- [45] M.-R. L. C. C. (MRLC), "National land cover database (nlcd)," 2021, accessed: 2024-03-01. [Online]. Available: <https://www.mrlc.gov/> 2

CAFOSat: A Strongly Annotated Dataset for Infrastructure-Aware CAFO Mapping Using High-Resolution Imagery

Supplementary Material

A. CAFOSat Overview.

An overview of the data processing pipeline is provided in Figure 2. The pipeline described in this section produces CAFOSat, a comprehensive, ML-ready dataset for CAFO detection and infrastructure mapping across the contiguous United States. The full dataset comprises **39,257 base image patches** (833×833 pixels, 0.6 m resolution) from 2023 NAIP imagery, spanning 20 U.S. states and six livestock categories (Swine, Poultry, Dairy, Beef, Horses, Sheep/Goats), plus 20,771 curated negative samples. An additional 6,454 synthetically augmented patches are included, bringing the total to approximately 45,000 patches. For each sample, CAFOSat provides:

- **Image patches:** High-resolution NAIP aerial imagery (833×833 px, 0.6 m/px) centered on CAFO or non-CAFO locations, organized by U.S. state.
- **Classification labels:** Facility-level CAFO type labels (Negative, Swine, Poultry, Dairy, Beef, Horses, Sheep/Goats) with human-verified and AI-annotated variants indicated via a `verified_label` flag.
- **Infrastructure-level annotations:** Binary flags for barn presence, manure pond presence, grazing area presence, and other infrastructure for 4,513 manually verified patches (see Table 2 for per-class counts).
- **Bounding box annotations:** Geospatial bounding boxes (`geom_bbox`) and polygon geometries (`geometry`) with associated coordinate reference systems for each patch.
- **Geospatial metadata:** Original weak coordinates (`weak_x`, `weak_y`) alongside refined coordinates (`refined_x`, `refined_y`), U.S. state, spatial resolution, and unique facility identifiers (`CAFO_UNIQUE_ID`).
- **Augmentation metadata:** For synthetic patches, the original source patch path, the inpainting prompt used, and the `image_type` flag distinguishing real from augmented samples.
- **Standardized splits:** Six pre-defined train/val/test split configurations (Verified, Augmented, Merged, Set 1, Set 2, All-Training) provided as boolean flags in the master metadata file (`CAFOSat.csv`), enabling reproducible benchmarking across different experimental setups (see Table 2).

The dataset is publicly available on HuggingFace¹ under a CC BY 4.0 license, with data loaders and processing scripts on GitHub². The remainder of this section details how each component is constructed.

B. Data Sources

Here, we provide a summary of data sources and acquisition. Details are in the supplement. Table S1 lists all data sources.

B.1. Satellite Imagery

We leverage aerial imagery from the National Agriculture Imagery Program (NAIP), accessed via the Microsoft Planetary Computer. For each geolocated CAFO point, the nearest cloud-free NAIP image is queried and downloaded using the STAC API. These images typically offer spatial resolutions between 60 cm and 1 m, depending on acquisition year and state. For this experimentation, we collected the most recent (2023) data for the studied states.

B.2. CAFO-Dataset

We collected CAFO location and corresponding cafo type primarily from two sources: (i) Department of Geographical and Sustainability Sciences of IOWA³ (denoted as IOWA-CAFO Inventory) and (ii) animal feeding operation report from states (denoted as State-CAFO Inventory).

IOWA-CAFO Inventory: This data inventory aggregates CAFO facility data from state environmental agencies across nine southeastern U.S. states: Alabama, Arkansas, Florida, Georgia, Louisiana, Mississippi, North Carolina, South Carolina, and Texas. Data is collected from permit databases, nutrient management plans, and agency inspections. Each record includes geolocation, animal type (poultry, swine, beef, dairy), and manure management details. While some states (e.g., Georgia, North Carolina) provide structured digital datasets, others require manual extraction from reports. This dataset standardizes these sources to enable regional CAFO distribution and impact analysis.

State-CAFO Inventory Several U.S. states publish CAFO reports curated by official state agencies using per-

¹<https://huggingface.co/datasets/oishee3003/CAFOSat>

²<https://github.com/oishee-hoque/CAFOSat>

³<https://cafomaps.org/>

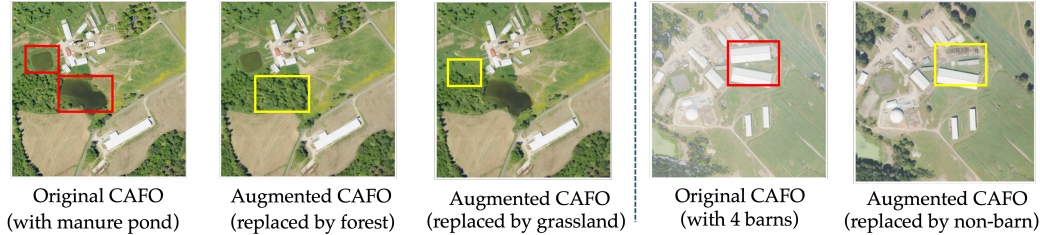


Figure S1. Examples from our augmented dataset. In the first example (left), the augmented images replace the manure pond with forest and grassland; in the second example (right), one barn is replaced with non-barn infrastructure. In both cases, the structural definition of the CAFO remains intact.

Table S1. Summary of Core CAFO Data Sources Used in Livestock Detection.

Source	Description	Use
NAIP Imagery (2023) [37]	High-resolution aerial imagery from the USDA National Agriculture Imagery Program	Visual input for CAFO patch extraction and model training
CAFOMaps [26]	Multi-state (i.e., Alabama, Arkansas, Florida, Georgia, Louisiana, Mississippi, North Carolina, South Carolina, and Texas) labeled dataset containing 6,604 CAFOs with animal type annotations (e.g., poultry, swine, beef, dairy), curated by IOWA researchers	Ground-truth labels for training and validation of CAFO classification models
State-CAFO Inventory [38–44]	Six independent data sources from official state-level CAFO registries corresponding to Indiana, Iowa, Maryland, Michigan, Minnesota, New York, and Delaware, curated from permit records, inspections, and nutrient management plans	Ground truth labels for ML-ready dataset
Land Use Masks (NLCD) [45]	National Land Cover Database (NLCD) used for masking agricultural zones	Used to create negative samples

mit records, inspection data, and self-reported nutrient management plans. Delaware’s CAFO report, maintained by the Socially Responsible Agricultural Project (SRAP), provides spatial boundaries and regulatory attributes for permitted operations. Indiana’s CAFO report, compiled by the Indiana Department of Environmental Management (IDEM), is publicly available via an ArcGIS map and contains metadata on facility type and permit status. Iowa’s inventory is provided by the Iowa Department of Natural Resources (Iowa DNR), offering geolocated animal feeding operations with supporting regulatory information. Maryland’s dataset is curated by the Maryland Department of the Environment (MDE), detailing registered CAFOs with geographic and operational metadata. Michigan’s CAFO data is managed by the Michigan Department of Environment, Great Lakes, and Energy (EGLE), covering operations across different time periods with detailed facility-level information. Additional inventories are available from the FracTracker Alliance and the New York Department of State (NYDOS), including permit identifiers and operator details across various temporal spans.

B.3. Land Use Masks (NLCD)

We utilize national-scale raster products to identify and contextualize agricultural areas. The MRLC National Land Cover Database (NLCD) offers 30m-resolution land cover classifications across 16 categories, including cultivated cropland, grassland, barren land, and pasture (See Table S1). This dataset is further used to generate stratified negative samples based on land cover types and spatial extent.

C. Additional Details for Section 3

Manual Verification Setup. Figure S2 visualizes the verification setup we used to manually verify and annotate the data.

Prompt Guided Data Augmentation To improve model generalization in CAFO infrastructure analysis, we develop a prompt-guided augmentation pipeline that removes visually identifiable structures, such as barns, manure ponds, and other supporting facilities. We then replace them with semantically plausible non-infrastructure content. This results in label-preserving image variants that diversify structural configurations while retaining the associated CAFO



Figure S2. Several Manual Verification and Labeling Setup

types (e.g., swine, dairy, poultry) as defined in the metadata. In total, 6454 samples were augmented using the following prompt-guided procedure (3921 involving barns, 1344 manure ponds, and 2089 other infrastructure elements):

- Infrastructure Detection via Vision-Language Prompts:** In this step our objective is to localize and identify physical structures within satellite imagery. Using GroundingDINO, a vision-language object detector, we detect infrastructure based on natural language prompts that encode high-level visual priors observed in overhead imagery. We carefully designed 25 prompts that capture geometric shape (e.g., rectangular, circular), material appearance (e.g., white roofs, dark water), and spatial context (e.g., isolated placement, proximity to buildings). For example, we use *“a long white rectangular building located in an open, unobstructed area”* for barn detection (see the Appendix Table S2). To ensure that prompts are grounded in semantically valid regions and to reduce spurious detections, we apply infrastructure detection only to patches where metadata confirms the presence of the corresponding structure. Note that the prompts are not intended to infer the facility’s animal type; rather, they target visual infrastructure elements that may appear across multiple CAFO categories. The prompts are all listed in Table S2.
- Inpainting for Structure Removal:** For structure removal, we generate binary masks from subsets of predicted bounding boxes (up to five per image) and use these to guide the removal of detected infrastructure. The RGB image and corresponding mask are passed to a Stable Diffusion Inpainting model, conditioned on non-

infrastructure prompts (e.g., “grassland”, “a small water pool”, “cluster of trees”). The model synthesizes contextually consistent content to fill the masked regions. To preserve the validity of the CAFO type label (e.g., swine, dairy, poultry), we remove infrastructure only when multiple instances are present within a patch. For example, if ten barns are detected, a subset (e.g., two or three) are removed to ensure the structural identity of the facility remains intact. This constraint prevents label ambiguity and preserves the semantic consistency of the augmented data. We also provide detailed metadata (including the number and type of structures removed, the inpainting prompt used, and the bounding box configuration) for each sample. This ensures full traceability and allows verification that label integrity is maintained across all synthetically generated samples.

This augmentation strategy introduces visual variation within the same semantic label, enabling models to generalize beyond repeated infrastructure patterns. By selectively removing structures while preserving the CAFO type, the model is encouraged to learn broader contextual features (e.g., landscape, vegetation, layout) rather than overfitting to infrastructure-specific cues.

D. Additional Details for Section 4

Training Setup. We trained all models using PyTorch on an NVIDIA A40 GPU with 40GB of memory. Training was conducted for a maximum of 30 epochs with early stopping (patience = 5) based on validation loss. We used a batch size of 32, a learning rate of 0.0001, and mixed-precision training (FP16) for improved efficiency. Each experiment used 12 data loading workers and was distributed across 2 GPUs where applicable. All models were trained on 8-class classification using the curated dataset described in Section 4.

Baseline Models In our benchmarking framework, we incorporate a diverse set of deep learning models to evaluate their effectiveness in both binary and multiclass CAFO classification tasks. We use ResNet18 and ResNet50 as strong convolutional baselines due to their proven reliability and computational efficiency. To explore transformer-based models, we include ViT-B/16 and Swin-B — with ViT offering global context understanding and Swin providing better spatial inductive biases through hierarchical attention. We also add EfficientNet-B0 and B3 for their state-of-the-art accuracy-efficiency tradeoffs, making them suitable for scalable deployment. Beyond these supervised architectures, we evaluate DINOv2-ViT-B, a self-supervised

Table S2. Grouped prompts and rationales for agricultural infrastructure types, with rationales structured by geometric shape, material appearance, and spatial context.

Structure	Prompt(s)	Rationale
Barn	a long white rectangular building located in an open, unobstructed area	Rectangular in shape with elongated dimensions, featuring light-colored roofs, and positioned in isolated, open fields with minimal surrounding structures.
	a large rectangular structure placed alone in a spacious open area	
	a light gray rectangular structure with a bright roof placed in a cleared field	Rectangular buildings with reflective or light-colored roofs, typically situated in uniform, cleared agricultural areas.
	a rectangular building with a reflective or light-colored roof in a uniform open setting	
	a simple white rectangular building with a flat or sloped roof surrounded by open land	Wide, low-profile rectangular shapes with simple white roofs, located far from roads or residential structures.
	a wide, low-rise building with a simple roof and no nearby roads or houses	
	a pale rectangular building that is isolated from other nearby structures	Box-shaped buildings with pale or white surfaces, spatially detached from other infrastructure in cleared zones.
	a white box-shaped building standing by itself in a cleared landscape	
	a long rectangular building with a white or gray roof and no surrounding clutter	Linear rectangular structures with white or gray roofing, placed in bare or uncluttered terrain.
	a linear structure with strong roof edges, positioned in an empty ground space	
Manure Pond	a dark brown or black irregular pond surrounded by open land	Irregularly shaped, dark-colored water bodies commonly located in bare land with limited vegetation or structures.
	a muddy or black spot on the ground surrounded by bare land	
	a small black water pool next to a large building	Dark, compact pools with irregular or circular shapes, typically near barns or placed away from residential zones.
	a dark patch of water placed away from houses or roads	
	a dark green or brown pool of water near agricultural buildings	Rectangular or rounded shapes with dark tones and low reflectance, often adjacent to farm structures.
	a rectangular dark spot with no reflection near farm infrastructure	
	a dirty water pond placed in a fenced or open farm area	Shallow, flat pits with dark water content, commonly found in fenced or exposed areas within farm boundaries.
a small flat black or brown pit in open space		
Other	a tall round silver structure standing alone in an open area	Cylindrical or rounded forms with metallic or reflective surfaces, typically isolated or aligned along roads or access routes.
	a silver or white round tank placed horizontally on the ground	
	a dark or metallic cylinder standing upright near a road or dirt track	Small rectangular or vertical pipe-like forms, white or neutral in appearance, located near barns or within farm complexes.
	a small box-shaped white structure placed near larger buildings	
	a narrow vertical pipe-like structure standing on open soil	Flat or elongated infrastructure lacking roofing, with metal or white coloring, typically positioned next to buildings.
	a flat structure with no roof, made of metal or concrete, placed near a building	
	a narrow white object placed across open soil with no walls or roof	Curved or residential-style structures with white exteriors and driveways, indicative of greenhouses or farmhouses.
	a small building with a curved roof sitting in a field	
a white rectangular building with windows and a driveway nearby		

vision transformer known for its strong generalization on downstream tasks. Finally, we integrate CLIP and RemoteCLIP, two vision-language models that offer zero-shot capability and strong representation learning without task-specific fine-tuning.

Evaluation Metrics To assess model performance, we use three complementary metrics: Accuracy, F1 Macro, and mean Average Precision (mAP). **Accuracy** measures the overall proportion of correct predictions across all classes but may be biased toward dominant classes in imbalanced datasets. To address this, we report **F1 Macro**, which com-

putes the F1 score independently for each class and averages them, giving equal weight to all classes regardless of frequency—making it especially important for evaluating performance on underrepresented CAFO types. Finally, we include **mean Average Precision (mAP)** to capture the precision-recall trade-off across thresholds, providing a robust indicator of class separability and detection quality. Together, these metrics offer a comprehensive view of model performance across both dominant and minority classes.

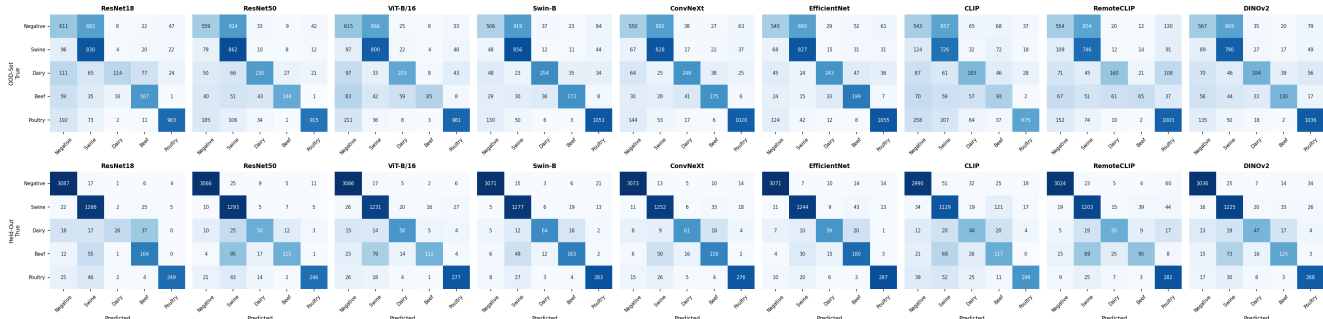


Figure S3. Confusion matrices for all nine models on the *Verified-Set* (*top row*) and *Held-Out Set* (*bottom row*), restricted to the five major classes. Cell values show raw counts; color intensity reflects row-normalized accuracy. Models perform substantially better on the in-distribution *Held-Out Set*. On the *Verified-Set*, *Negative* samples are frequently misclassified as *Swine*, and *Dairy* and *Beef* show persistent mutual confusion due to visual similarity. *Poultry* is the easiest class to recognize across both sets, owing to its visually distinct long-barn infrastructure.

Model	Negative	Barn	Manure Pond	Grazing Area	Other Infra.
CLIP	0.432	0.505	0.414	0.313	0.689
ConvNeXt-Tiny	0.406	0.589	0.494	0.563	0.825
DINOv2-ViT-B	0.461	0.573	0.511	0.542	0.808
EfficientNet-B0	0.463	0.593	0.618	0.593	0.863
RemoteCLIP	0.465	0.515	0.385	0.343	0.717
ResNet18	0.473	0.584	0.558	0.536	0.831
ResNet50	0.464	0.611	0.579	0.574	0.842
Swin-B	0.496	0.596	0.571	0.563	0.854
ViT-B/16	0.483	0.591	0.593	0.546	0.836

Table S3. Per-class F1 scores for infrastructure-level detection across all evaluated models, computed on the *Verified Set*. Each model is trained on the Standard Training Set and evaluated on binary presence/absence of barn, manure pond, grazing area, and other infrastructure within manually annotated CAFO patches. Bold values indicate the best per-column performance.